A variable order hidden Markov model with dependence jumps

Anastasios Petropoulos, Stelios Xanthopoulos, and Sotirios P. Chatzis

***Abstract*—Hidden Markov models (HMMs) are a popular approach for modeling sequential data, typically based on the assumption of a first- or moderate-order Markov chain. However, in many real-world scenarios the modeled data entail temporal dynamics the patterns of which change over time. In this paper, we address this problem by proposing a novel HMM formulation, treating temporal dependencies as latent variables over which inference is performed. Specifically, we introduce a hierarchical graphical model comprising two hidden layers: on the first layer, we postulate a chain of latent observation-emitting states, the temporal dependencies between which may change over time; on the second layer, we postulate a latent first-order Markov chain modeling the evolution of temporal dynamics (dependence jumps) pertaining to the first-layer latent process. As a result of this construction, our method allows for effectively modeling non-homogeneous observed data, where the patterns of the entailed temporal dynamics may change over time. We devise efficient training and inference algorithms for our model, following the expectation-maximization paradigm. We demonstrate the efficacy and usefulness of our approach considering several real-world datasets. As we show, our model allows for increased modeling and predictive performance compared to the alternative methods, while offering a good trade-off between the resulting increases in predictive performance and computational complexity.**

***Index Terms*—Temporal dynamics; hidden Markov models; expectation-maximization; variable order; dependence jumps.**

I. Introduction

Modeling sequential data continues to be a fundamental task and a key challenge in the field of machine learning, encountered in a plethora of real-world applications, including bioinformatics, document analysis, financial engineering, speech processing, and computer vision, to name just a few. In this paper, we focus on the problem of *sequence prediction*, dealing with *continuous*, possibly *high-dimensional* observations (time-series). Machine learning literature comprises a rather extensive corpus of proposed prediction algorithms for sequences of continuous observations. Among them, the hidden Markov model (HMM) is one of the most popular methods, used in a great variety of application contexts. This popularity is mainly due to the fact that HMMs are flexible enough to allow for modeling complex temporal patterns and structures in sequential data. Specifically, HMMs are popular for their provision of a convenient way of modeling observations appearing in a sequential manner and tending to cluster or to alternate between different possible components (subpopulations) [1].

Most popular HMM formulations are based on the postulation of first-order Markovian dependencies; in other words, only one-step-back temporal dynamics are considered. Such an assumption allows for increased simplicity and low computational complexity of the resulting model training and inference algorithms. However, postulating first-order temporal dynamics does also entail ignoring the possibility of the modeled data comprising longer temporal dynamics. Even though this assumption might be valid in some cases, it is well-known to be unrealistic in several application scenarios, including handwriting recognition, molecular biology, speech recognition, and volatility prediction in financial return series, thus undermining the modeling effectiveness.

To resolve this problem, several researchers have attempted to introduce HMM-type models with higher-order dependencies. Characteristic examples are the methods presented in [2] and [3], with successful applications to the problem of speech recognition, the method presented in [4], applied to handwriting recognition, the method of [5], designed to address challenges related to pattern recognition tasks in molecular biology, and the method presented in [6], which was successfully applied to the field of robotics. However, a major drawback of such higher-order HMM approaches is their considerably increased computational costs, which become rather prohibitive as model order increases. An effort to ameliorate these issues of higher-order HMMs is presented in [7]. In that work, instead of directly training R-th order HMMs on the data, a method of fast incremental training is used that progressively trains HMMs from first to R-th order.

Note, though, that using higher-order HMMs gives rise to a source of significant burden for researchers and practitioners, namely the need to determine the most appropriate order for the postulated models. This procedure entails fitting multiple models to the available data to choose from, and application of some cross-validation procedure, which, apart from computationally cumbersome, is also likely to become prone to overfitting [8]. Finally, another limitation of the existing higher-order HMM formulations concerns their static and homogeneous assumptions, i.e. their consideration that the temporal dynamics order in the modeled data does not change over time. Indeed, sequential data with variable order in the entailed temporal dynamics are quite often encountered in real-world application scenarios [9], [10], [11], [12]. Therefore, allowing for capturing more complex structure of temporal dynamics in the modeled data, where effective model order may change over time as a result of dynamic switching between different temporal patterns, is expected to result in much better modeling and predictive performances. Indeed, previous works such as [13] and [14] have proven the efficacy of postulating simple variable-order Markov chains in diverse application settings. However, development of a variable-order

HMM-type model has not yet been considered in the literature.

To address these problems of conventional higher-order HMMs, some researchers have proposed appropriate models with variable order Markovian dynamics assumptions. For instance, a variable order Markov model is presented in [10] to address the problem of prediction of discrete sequences over a finite alphabet; the method is successfully applied to three different domains, namely English text, music pieces, and proteins (amino-acid sequences). More recently, [11] presented a simple and effective generalization of variable order Markov models to full online Bayesian estimation. Generalization of variable order Markov models in this context enables perpetual model improvement and enrichment of the learned temporal patterns by accumulation of observed data, without any need for human intervention. Despite these merits, a drawback of both these approaches concerns their inability to model sequential data comprising continuous observations, i.e. sequences each frame of which is a (probably high-dimensional) D-dimensional vector of real values, defined in $\mathbb{R}^D$. Finally, [15] propose a two-stage modeling approach towards variable order HMMs: the first stage consists in discovering repetitive temporal patterns of variable length, while the second stage consists in performing prediction by means of a separate simple HMM fit to the temporal pattern determined to be relevant at each specific time point. Similar to the previous approaches, a major limitation of [15] consists in its incapability to model sequential observations taking *continuous* values in $\mathbb{R}^D$.

In this paper, we address the aforementioned shortcomings, by introducing an HMM variant capable of capturing *jumps* in the temporal *dependence patterns* of modeled sequential data. Specifically, we introduce a hierarchical graphical model comprising two hidden layers: on the *first layer*, we postulate a *chain* of *latent observation-emitting states,* the *dependencies* between which may *change over time*; on the *second layer,* we postulate a *latent first-order Markov chain* modeling the *evolution* of temporal dynamics (*dependence jumps*) pertaining to the first-layer latent process. As a result of this construction, our model allows for effectively modeling non-homogeneous observed data, where the patterns of temporal dependencies may change over time. To allow for tractable training and inference procedures, our model considers *temporal dependencies* taking the form of *variable order dependence jumps*, the order of which is *inferred* from the data as part of the model inference procedure.

Our method is designed to allow for modeling *both* discrete and continuous observations; it allows for capturing seasonal effects in the modeled sequences, and enhances modeling in the implied autocorrelation structure of the observed sequences. In addition, contrary to the related methods of [9] and [12], our method does *not* require utilization of any kind of approximation to perform model training and inference. Indeed, both model training and inference can be performed *exactly* and in a computationally efficient way, using elegant algorithms derived under the expectation-maximization paradigm [16]. We demonstrate the efficacy of our approach considering real-world application scenarios.

The remainder of this paper is organized as follows: In Section II, we introduce our proposed model and derive its training and inference algorithms. In Section III, we experimentally evaluate our approach, and exhibit its advantages over existing approaches. Finally, in Section IV we conclude this paper, summarizing and discussing our results.

II. Proposed Approach

A. Motivation

In real-world applications, it is often the case that stochastic processes are characterized by non-homogeneous evolution, exhibiting higher-order dependencies. For example, time series of financial asset returns are known to exhibit variable autocorrelation and non-stationarity [17]; such forms of dynamics in the modeled data cannot be sufficiently captured by using a simple Markov process. In the same vein, historical volatility of financial asset returns usually exhibits long temporal interdependencies, slow autocorrelation decay, fat distribution tails, as well as temporal pattern switching over time, e.g. shifting between low volatility and high volatility regimes [18], [19], [20], [21], which are manifested as jumps driven by shocks or unexpected news [22], [23].

Several studies have examined whether conventional HMM formulations are capable of capturing such stylized facts in modeled time-series. For example, [24] examined the efficacy of simple first-order HMMs; further, [25] used hidden semi-Markov models (HSMMs) as an alternative solution allowing for better capturing the autocorrelation structure. However, the outcome of all these studies has been quite unsatisfactory compared to the state-of-the-art in the literature pertaining to the related applications, e.g. the literature on financial return series modeling. Motivated from these results, in this work we aim to come up with an elegant and computationally efficient HMM variant capable of accommodating the above-mentioned stylized facts in observed time-series, namely: (i) distributions with fat tails; (ii) seasonality and temporal clustering dynamics; and (iii) non-homogeneous temporal dynamics patterns, exhibiting dependence jumps over time.

B. Model Definition

As we have already discussed, in this work we are seeking to devise an HMM variant allowing for modeling sequential data with *variable temporal dependence patterns*, i.e. a model capable of determining *dependence jumps* in the chain of observation-emitting latent states. For this purpose, we postulate an HMM variant, the hierarchical construction of which comprises *two hidden layers*: The *first layer* essentially consists of the chain of *observation-emitting* latent states, the dependencies between which may *change form* over time. The *second layer* comprises a latent *first-order Markov chain* that determines (and generates) the *dependence jumps* taking place in the observation-emitting latent chain of the first layer.

Let us postulate N observation-emitting states on the chain of the first layer of our model, where the hidden emission density of each state is modeled by a M-component finite mixture model. Let us also postulate a latent first-order Markov chain comprising K states on the second layer; K is essentially the number of alternative temporal dependence patterns considered on the first layer of the model. Even though multiple

alternative configurations could be considered for the form of the modeled temporal dependence patterns of the first-layer observation-emitting chain, in this work we limit ourselves to pairwise latent emitting state transitions between the *current* emitting state and *some previous state that occurred at a time point a number of steps back;* this number of steps back is determined from the latent values generated from the *second-layer dependence jumps-generating Markov chain* of our model.

Let us introduce here some useful notation. We denote as $O = \{\boldsymbol{o}_t\}_{t=1}^T$ an observed data sequence, with $\boldsymbol{o}_t \in \mathbb{R}^D$. The latent (unobserved) data associated with this sequence comprise: (i) the corresponding *emitting state* sequence $Q = \{q_t\}_{t=1}^T$, where $q_t = 1, \ldots, N$ is the indicator of the state the tth observation is emitted from; (ii) the sequence of *temporal dependence form* indicators $Z = \{z_t\}_{t=1}^T$ that indicate the pairwise emitting states transition that is relevant ("active") at time t, where $z_t = 1, \ldots, K$; and (iii) the sequence of the corresponding *mixture component* indicators $L = \{l_t\}_{t=1}^T$, where $l_t = 1, \ldots, M$ indicates the mixture component density that generated the tth observation. A graphical illustration of the generative model and the latent interdependencies assumptions of our model is provided in Fig. 1.

The above-described model comprises the set of parameters $\Theta = \{\Phi, \Psi\}$, where Φ denotes the parameters set of the emission distributions of the model, and Ψ denotes the set of parameters of the postulated latent processes pertaining to the observed data dynamics (first-layer process) and the dependence jump dynamics (second-layer process). Specifically, since the second-layer process is a simple first-order Markov chain, it comprises the parameters

$$\hat{\varpi}_k \triangleq p(z_1 = k) \tag{1}$$

that denote the (prior) probabilities of the initial state of this Markov chain, and the parameters

$$\hat{\pi}_{kk'} = p(z_t = k' | z_{t-1} = k) \; \forall t > 1 \tag{2}$$

denoting the transition (prior) probabilities of this Markov chain. From the above model definition, we observe that, if the transition probability $\hat{\pi}_{11}$ in the above-defined transition matrix $\hat{\boldsymbol{\Pi}} \triangleq [\pi_{kk'}]_{k,k'}$ is close to one, then the observation-emitting process of our model (first model layer) almost reduces to a first-order Markov chain. In this paper, for simplicity we set $\hat{\varpi}_k = \frac{1}{K} \; \forall k$ and $\hat{\pi}_{kk'} = \frac{1}{K} \; \forall k, k'$; in other words, we consider all dependence forms a priori of equal probability. These assumptions, although relatively limiting, allow for deriving tractable and computationally efficient model training and inference algorithms, as we show further on.

In a similar fashion, the postulated first-layer process of our model comprises the parameters

$$\varpi_i \triangleq p(q_1 = i) \tag{3}$$

denoting the (prior) probabilities of the initial observation-emitting state, with $\boldsymbol{\varpi} \triangleq [\varpi_i]_{i=1}^N$. In addition, turning to the variable-form temporal dynamics of this process, we also introduce the set of *dependence form-conditional* transition (prior) probability matrices $\{\boldsymbol{\Pi}^k\}_{k=1}^K$, with

$$\boldsymbol{\Pi}^k \triangleq [\pi_{ij}^k]_{i,j=1}^N \tag{4}$$

where

$$\begin{aligned} \pi_{ij}^k \triangleq & p(q_t = j | q_{t-1}, \ldots, q_{t-k} = i; z_t = k) \\ & = p(q_t = j | q_{t-k} = i; z_t = k) \end{aligned} \tag{5}$$

In other words, we consider different (pairwise) state transition probabilities, depending on the inferred dependence form k (number of steps back) generated from the postulated second-layer process. By limiting hidden state dependence to pairwise interactions, as described in (5), we facilitate tractability of the inference algorithms of our model, without restricting its modeling power in a harmful manner. Indeed, this is the case in many scientific fields, e.g. in finance, where it is well-understood that temporal dynamics tend to be dominated (at each time point) by one specific past state [26], [21].

Having defined the latent processes of our model, with effective parameters set $\Psi = \left\{\boldsymbol{\varpi}, \{\boldsymbol{\Pi}^k\}_{k=1}^K\right\}$, we can now proceed to the definition of the (conditional on the first-layer states) emission distributions of our model. In this work, we focus on modeling continuous-valued observations; for this reason, we postulate M-component finite mixture models, as we have already discussed. Specifically, *to also allow for modeling distributions with fat tails,* we consider two alternative selections: (i) multivariate Gaussian mixture models, yielding

$$p(\boldsymbol{o}_t | q_t = i) = \sum_{m=1}^M w_{im} \mathcal{N}(\boldsymbol{o}_t | \boldsymbol{\mu}_{im}, \boldsymbol{\Sigma}_{im}) \tag{6}$$

where $\mathcal{N}(\cdot | \boldsymbol{\mu}, \boldsymbol{\Sigma})$ is a multivariate Gaussian with mean $\boldsymbol{\mu}$ and covariance matrix $\boldsymbol{\Sigma}$, while $\{w_{im}\}_m$ is the set of mixture component weights of the $q_t = i$ state; and (ii) multivariate Student's-t mixture models, yielding

$$p(\boldsymbol{o}_t | q_t = i) = \sum_{m=1}^M w_{im} \mathcal{S}(\boldsymbol{o}_t | \boldsymbol{\mu}_{im}, \boldsymbol{\Sigma}_{im}, \nu_{im}) \tag{7}$$

where $\mathcal{S}(\cdot | \boldsymbol{\mu}, \boldsymbol{\Sigma}, \nu)$ is a multivariate Student's-t distribution with parameters $\boldsymbol{\mu}$, $\boldsymbol{\Sigma}$, and ν degrees of freedom. On this basis, the parameters set Φ yields $\Phi = \{w_{im}, \boldsymbol{\mu}_{im}, \boldsymbol{\Sigma}_{im}\}_{i,m}$ or $\Phi = \{w_{im}, \boldsymbol{\mu}_{im}, \boldsymbol{\Sigma}_{im}, \nu_{im}\}_{i,m}$, respectively. As discussed in [27], HMM-type models with Student's-t mixture emission distributions allow for better modeling sequential data stemming from populations with long tails, which are quite common in real-world application scenarios. Note that these assumptions do not harm the generality of our approach. Modeling discrete-valued sequences can be performed in a straightforward way, by simply postulating multinomial conditional distributions instead of the finite mixture models in (6)-(7).

This concludes the definition of our model. We dub our approach the variable dependence jump HMM (VDJ-HMM). From Eqs. (1)-(7), the joint distribution of VDJ-HMM yields:

$$p(O, Q, Z | \Theta) = \hat{\varpi}_{z_1} \varpi_{q_1} \prod_{t=1}^{T-1} \hat{\pi}_{z_t, z_{t+1}} \prod_{t>1} \pi_{q_{t-z_t}, q_t}^{z_t} \prod_{t=1}^T p(\boldsymbol{o}_t | q_t = i) \tag{8}$$

Note that, as observed from (8), a major advantage from

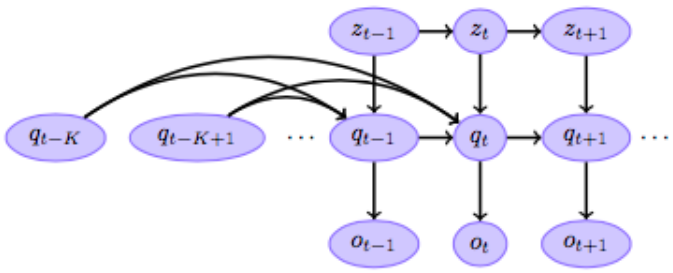

Figure 1: Graphical illustration of the generative model and the latent interdependencies assumptions of VDJ-HMM.

the computational point of view of the proposed VDJ-HMM model compared to higher-order HMM formulations (e.g., [2], [6], [7]) is the much fewer number of parameters postulated from VDJ-HMM. As a result, VDJ-HMM is capable of capturing seasonal effects in the modeled data while allowing for significantly more efficient training and inference algorithms compared to existing alternatives. In addition, the lower number of trainable parameters reduces the tendency of the model to overfitting, as well as the associated requirements in training data availability to ensure effective model training.

C. Model Training

To perform training for our model given a sequence $O = \{\boldsymbol{o}_t\}_{t=1}^T$, we resort to the familiar expectation-maximization (EM) paradigm [generalization of the here-derived algorithm for the case of training with multiple sequences is straightforward]. Based on the definition of VDJ-HMM [Eqs. (1)-(7)], the complete data of our model comprise the observable sequence O, the corresponding emitting state sequence $Q = \{q_t\}_{t=1}^T$, the dependence form sequence $Z = \{z_t\}_{t=1}^T$, and the sequence of corresponding mixture component indicators $L = \{l_t\}_{t=1}^T$. In addition, based on the derivations of [27], in the special case of considering multivariate Student's-t mixture models as the emission distributions of VDJ-HMM, to allow for effective model training and inference procedures, we resort to expressing the multivariate Student's-t distributions as scale-mixtures of Gaussians, yielding [27]:

$$p(\boldsymbol{o}_t|q_t = i; \{u_{imt}\}_{m=1}^M) = \sum_{m=1}^M w_{im}\mathcal{N}(\boldsymbol{o}_t; \boldsymbol{\mu}_{im}, \boldsymbol{\Sigma}_{im}/u_{imt}) \tag{9}$$

where u_{imt} is a precision scalar corresponding to the observation $\boldsymbol{o}_t$ given it is generated from the jth component density of the ith emitting state, and is Gamma-distributed as [27]

$$u_{imt} \sim \mathcal{G}\left(\frac{\nu_{im}}{2}, \frac{\nu_{im}}{2}\right) \tag{10}$$

Under this setup, the above introduced set of precision scalars $\{u_{imt}\}$ is also regarded as part of the complete data configuration of our model.

The EM algorithm comprises optimization of the posterior expectation of the complete data log-likelihood of the treated model [16]

$$Q(\Theta; \hat{\Theta}) \triangleq E_{\hat{\Theta}}(\log L_c(\Theta)|O) \tag{11}$$

where $\hat{\Theta}$ denotes the currently obtained estimator of the model parameters set Θ, and $\log L_c(\Theta)$ is the expression of the complete data log-likelihood of the model, which reads (ignoring constant terms)

$$\begin{aligned}\log L_c(\Theta) = \sum_{h=1}^N \Bigg\{ &\mathbb{I}[q_1 = h]\, \log\varpi_h \\ &+ \sum_{k=1}^K \sum_t \mathbb{I}[z_t = k] \sum_{i=1}^N \mathbb{I}[q_{t-k} = h,\ q_t = i]\, \log\pi_{hi}^k \Bigg\} \\ &+ \sum_{t=1}^T \sum_{i=1}^N \mathbb{I}[q_t = i] \log L_c(\boldsymbol{o}_t|q_t = i)\end{aligned} \tag{12}$$

where $\mathbb{I}[\cdot]$ is the boolean operator. In Eq. (12), $\log L_c(\boldsymbol{o}_t|q_t = i)$ is the complete data log-likelihood of the emission distribution of the ith hidden state with respect to $\boldsymbol{o}_t$, and the associated latent variables l_t and (in case of Student's-t models) $\{u_{imt}\}_m$. In the case of Gaussian mixture emission distributions, $\log L_c(\boldsymbol{o}_t|q_t = i)$ yields

$$\begin{aligned}\log L_c(\boldsymbol{o}_t|q_t = i) = \sum_{m=1}^M \mathbb{I}[l_t = m] \Bigg\{ &\log w_{im} - \frac{1}{2}\log|\boldsymbol{\Sigma}_{im}| \\ &- \frac{1}{2} d(\boldsymbol{o}_t, \boldsymbol{\mu}_{im}; \boldsymbol{\Sigma}_{im}) \Bigg\}\end{aligned} \tag{13}$$

where $d(\boldsymbol{o}_t, \boldsymbol{\mu}_{im}; \boldsymbol{\Sigma}_{im})$ is the Mahalanobis distance between $\boldsymbol{o}_t$ and $\boldsymbol{\mu}_{im}$, with covariance matrix $\boldsymbol{\Sigma}_{im}$. On the other hand, in the case of Student's-t mixture emission distributions, $\log L_c(\boldsymbol{o}_t|q_t = i)$ yields

$$\begin{aligned}\log L_c(\boldsymbol{o}_t|q_t = i) = \sum_{m=1}^M \mathbb{I}[l_t = m] \Bigg\{ &-\log\Gamma\left(\frac{\nu_{im}}{2}\right) + \frac{\nu_{im}}{2} \times \\ &\left[\log\left(\frac{\nu_{im}}{2}\right) + \log u_{imt} - u_{imt}\right] + \log w_{im} \\ &- \frac{u_{imt}}{2} d(\boldsymbol{o}_t, \boldsymbol{\mu}_{im}; \boldsymbol{\Sigma}_{im}) - \frac{1}{2}\log|\boldsymbol{\Sigma}_{im}| \Bigg\}\end{aligned} \tag{14}$$

where $\Gamma(\cdot)$ is the Gamma function.

As usual, the EM algorithm for our model is an iterative procedure, each iteration of which comprises an E-step and an M-step. On the E-step of the algorithm, we compute a set of posterior expectations pertaining to the latent variables of our model (sufficient statistics), using the current estimator of the model parameters set $\hat{\Theta}$. Subsequently, on the M-step of the algorithm, we optimize the model parameters set Θ using the sufficient statistics computed previously, in order to obtain an updated estimator of the model parameters set, $\hat{\Theta}$.

1) E-step: From (11) and (12), it directly follows that the E-step of our algorithm consists in computing the posterior probabilities of the latent states on the first and second hidden layers of our model, as well as the corresponding state transition posteriors. It also comprises computation of the emitting state-conditional mixture component posteriors, as well as the posteriors of the precision scalars u_{imt}, when considering Student's-t mixture emission distributions.

Let us begin with the mixture component posteriors, hereafter denoted as ξ_{imt}; we have

$$\xi_{imt} \triangleq E_{\Theta}(l_t = m|\boldsymbol{o}_t, q_t = i) = \frac{p(\boldsymbol{o}_t|q_t = i, l_t = m)}{\sum_{h=1}^{M} p(\boldsymbol{o}_t|q_t = i, l_t = h)} \tag{15}$$

This expression yields

$$\xi_{imt} = \frac{w_{im}\mathcal{N}(\boldsymbol{o}_t|\boldsymbol{\mu}_{im}, \boldsymbol{\Sigma}_{im})}{\sum_{h=1}^{M} w_{ih}\mathcal{N}(\boldsymbol{o}_t|\boldsymbol{\mu}_{ih}, \boldsymbol{\Sigma}_{ih})} \tag{16}$$

when considering Gaussian mixture emissions, and

$$\xi_{imt} = \frac{w_{im}\mathcal{S}(\boldsymbol{o}_t|\boldsymbol{\mu}_{im}, \boldsymbol{\Sigma}_{im}, \nu_{im})}{\sum_{h=1}^{M} w_{ih}\mathcal{S}(\boldsymbol{o}_t|\boldsymbol{\mu}_{ih}, \boldsymbol{\Sigma}_{ih}, \nu_{ih})} \tag{17}$$

in the case of Student's-t mixture emissions.

Regarding the posterior expectations of the precision scalars u_{imt} (if applicable), we have

$$\hat{u}_{imt} \triangleq E_{\Theta}\left(u_{imt}|\boldsymbol{o}_t\right) = \frac{\nu_{im} + D}{\nu_{im} + d(\boldsymbol{o}_t, \boldsymbol{\mu}_{im}; \boldsymbol{\Sigma}_{im})} \tag{18}$$

Further, to obtain the rest of the sought posteriors, we need to define a set of auxiliary distributions, which can be computed by means of a variant of the well-known forward-backward algorithm [28], [1]. Specifically, let us define the forward probabilities

$$\alpha_t(i,k) \triangleq p(\{\boldsymbol{o}_\tau\}_{\tau=1}^{t}, q_t = i|z_t = k) \tag{19}$$

These probabilities can be computed iteratively, with initialization

$$\alpha_1(i,k) = \begin{cases} \varpi_i p(\boldsymbol{o}_1|q_1 = i), k = 1 \\ 0, k > 1 \end{cases} \tag{20}$$

and recursion

$$\begin{aligned} \alpha_t(j,k) =& p(\boldsymbol{o}_t|q_t = j) \sum_{q_{t-k}} \pi_{q_{t-k},j}^{k} \sum_{q_{t-1}} \sum_{z_{t-1}} \hat{\pi}_{z_{t-1},z_t} \\ & \times \alpha_{t-1}(q_{t-1}, z_{t-1}) \end{aligned} \tag{21}$$

In a similar way we define the backward probabilities of our model, which yield

$$\beta_t(i,k) \triangleq p(\{\boldsymbol{o}_\tau\}_{\tau=t+1}^{T}|q_t = i; z_{t+k} = k) \tag{22}$$

These probabilities can also be computed iteratively, with initialization

$$\beta_T(i,k) = 1, \ \forall k \tag{23}$$

and recursion

$$\begin{aligned} \beta_t(i,k) =& \sum_{q_{t+k}} \pi_{i,q_{t+k}}^{k} p(\boldsymbol{o}_{t+k}|q_{t+k}) \sum_{q_{t+1}} \sum_{z_{t+1}} \hat{\pi}_{z_t,z_{t+1}} \\ & \times \beta_{t+1}(q_{t+1}, z_{t+1}) \end{aligned} \tag{24}$$

Having obtained the forward and backward probabilities of our model, we can now proceed to obtain the remaining sought posteriors. For the emitting state posteriors, hereafter denoted as γ_{jt}, we have

$$\gamma_{jt} \triangleq p(q_t = j|O) \propto \left[\sum_{k=1}^{K} \zeta_{kt}\alpha_t(j,k)\right]\left[\sum_{k'=1}^{K} \zeta_{k',t+k'}\beta_t(j,k')\right] \tag{25}$$

Similarly, the emitting state transition posteriors yield

$$\begin{aligned} \gamma_{ijt}^{\lambda} \triangleq& p(q_t = i, q_{t+\lambda} = j|Z; O) \\ \propto& \sum_{k,k'=1}^{K} \alpha_t(i,k)\beta_{t+\lambda}(j,k')\pi_{ij}^{\lambda} p(\boldsymbol{o}_{t+\lambda}|q_{t+\lambda} = j) \end{aligned} \tag{26}$$

Finally, regarding the ("active") dependence form posteriors, hereafter denoted as ζ_{kt}, we have

$$\zeta_{kt} \triangleq E(z_t = k|O) \propto \sum_{i} \alpha_t(i,k)\beta_t(i,k) \tag{27}$$

This concludes the E-step of our algorithm.

2) M-step: Having obtained the required posterior expectation expressions on the E-step of the training algorithm of our model, we now proceed to optimization of the objective function (11) over the model parameters to obtain the expressions of the model parameter updates. Let us introduce the notation

$$r_{imt} \triangleq \gamma_{it}\xi_{imt} \tag{28}$$

We then have

$$\pi_i = \gamma_{i1} \tag{29}$$

$$\pi_{hi}^{\lambda} = \frac{\sum_t \gamma_{hit}^{\lambda}}{\sum_t \gamma_{ht}} \tag{30}$$

$$w_{im} = \frac{\sum_{t=1}^{T} r_{imt}}{\sum_{t=1}^{T} \gamma_{it}} \tag{31}$$

Further, the parameters of the emission distributions yield the following expressions:

(i) In case of Gaussian mixture emissions, we have

$$\boldsymbol{\mu}_{im} = \frac{\sum_{t=1}^{T} r_{imt}\boldsymbol{o}_t}{\sum_{t=1}^{T} r_{imt}} \tag{32}$$

$$\boldsymbol{\Sigma}_{im} = \frac{\sum_{t=1}^{T} r_{imt}(\boldsymbol{o}_t - \boldsymbol{\mu}_{im})(\boldsymbol{o}_t - \boldsymbol{\mu}_{im})^T}{\sum_{t=1}^{T} r_{imt}} \tag{33}$$

(ii) In case of Student's-t mixture emissions, we have

$$\boldsymbol{\mu}_{im} = \frac{\sum_{t=1}^{T} r_{imt}\hat{u}_{imt}\boldsymbol{o}_t}{\sum_{t=1}^{T} r_{imt}\hat{u}_{imt}} \tag{34}$$

$$\boldsymbol{\Sigma}_{im} = \frac{\sum_{t=1}^{T} r_{imt}\hat{u}_{imt}(\boldsymbol{o}_t - \boldsymbol{\mu}_{im})(\boldsymbol{o}_t - \boldsymbol{\mu}_{im})^T}{\sum_{t=1}^{T} r_{imt}} \tag{35}$$

while the degrees of freedom are obtained by solving w.r.t. ν_{im} the equation

$$\begin{aligned} & 1 - \psi\left(\frac{\nu_{im}}{2}\right) + \log\left(\frac{\nu_{im}}{2}\right) \\ & + \psi\left(\frac{\hat{\nu}_{im} + D}{2}\right) - \log\left(\frac{\hat{\nu}_{im} + D}{2}\right) \\ & + \frac{1}{\sum_{t=1}^{T} r_{imt}} \sum_{t=1}^{T} r_{imt}\left(\log\hat{u}_{imt} - \hat{u}_{imt}\right) = 0 \end{aligned} \tag{36}$$

where $\hat{\nu}_{im}$ is the current estimate of the degrees of freedom ν_{im}, and $\psi(\cdot)$ is the Digamma function.

This concludes the training algorithm of our model. An outline of the EM algorithm for VDJ-HMM is provided in Alg. 1.

Algorithm 1 EM Algorithm for the VDJ-HMM model.

Initialize the model parameters estimate $\hat{\Theta}$. Set the maximum number of iterations, $MAXITER$, and the convergence threshold of the EM algorithm.
For $MAXITER$ iterations or until convergence of the objective function $Q(\Theta;\hat{\Theta})$ **do**:

1) Conduct the forward-backward algorithm to obtain the forward probabilities $\alpha_t(j,k)$ and the backward probabilities $\beta_t(i,k)$, using Eqs. (20)-(21) and (23)-(24), respectively.
2) Effect the E-step of the algorithm by computing the posteriors pertaining to the mixture components, ξ_{imt}, the precision scalars, $\hat{u}_{imt}$, the chain of observation-emitting states, γ_{jt} and γ^{λ}_{ijt}, and the Markov chain of dependence jumps, ζ_{kt}. For this purpose, use Eqs. (15), (18), (25)-(26), and (27), respectively.
3) Effect the M-step by computing the new estimates of the model parameters π_i, π^{λ}_{hi}, w_{im}, $\boldsymbol{\mu}_{im}$, $\boldsymbol{\Sigma}_{im}$, and ν_{im}, using Eqs. (29)-(36), respectively.

D. Inference Algorithm

A first inference problem we consider in this work is the problem of predicting the next emitting state, say at time $t+1$, denoted as q_{t+1}, given the values of the currently observed data, i.e. the observations set $\{\boldsymbol{o}_\tau\}_{\tau=1}^{t}$. From the definition of our model, it is easy to deduce that the probability of the emitting state at time $t+1$, given the sequence of past observations $\{\boldsymbol{o}_\tau\}_{\tau=1}^{t}$, can be written in the form

$$\begin{aligned} p(q_{t+1}=j|\{\boldsymbol{o}_\tau\}_{\tau=1}^{t}) &= \sum_{k}\sum_{i=1}^{N} p(q_{t-k+1}=i|\{\boldsymbol{o}_\tau\}_{\tau=1}^{t}) \\ &\quad \times p(q_{t+1}=j|q_{t-k+1}=i;z_{t-k+1}=k) \\ &= \sum_{k}\sum_{i=1}^{N} \pi^{k}_{ij}\gamma_{i,t-k+1} \end{aligned} \tag{37}$$

where the emitting state posteriors γ_{jt} are computed by (25), using the sequence of observations $\{\boldsymbol{o}_\tau\}_{\tau=1}^{t}$. On this basis, determination of the first-layer state of our model, say $\hat{q}$, that is most likely to emit the (next) observation at time $t+1$ can be performed by maximization of the conditionals $p(q_{t+1}=j|\{\boldsymbol{o}_\tau\}_{\tau=1}^{t})$, yielding:

$$\hat{q} \triangleq \underset{j}{\operatorname{argmax}}\; p(q_{t+1}=j|\{\boldsymbol{o}_\tau\}_{\tau=1}^{t}) \tag{38}$$

Another inference problem quite common in the related literature is the task of determining the probability of a given sequence w.r.t. a trained VDJ-HMM model. For this purpose, we can resort to the forward algorithm of our model, similar to conventional HMMs. Specifically, let us consider a sequence $O=\{\boldsymbol{o}_t\}_{t=1}^{T}$ and a trained VDJ-HMM model with parameter estimate $\hat{\Theta}$. Then, following the definition of our model, the probability of sequence O w.r.t. the available VDJ-HMM model yields

$$p(O|\hat{\Theta}) = \sum_{i=1}^{N}\sum_{k=1}^{K}\alpha_T(i,k) \tag{39}$$

Table I: EUR-USD exchange rate volatility: Optimal VDJ-HMM model configuration.

Parameter	Value
K	4
N	2
M	3

Finally, as discussed in the Introduction, the key *inference* problem we focus on in this work is the problem of *sequence prediction*. Let us consider a sequence $\{\boldsymbol{o}_\tau\}_{\tau=1}^{t}$. Then, the sequence prediction problem we consider here is the problem of performing an one-step ahead forecast, i.e. predicting the observation value $\boldsymbol{o}_{t+1}$ at time $t+1$, given the values $\{\boldsymbol{o}_\tau\}_{\tau=1}^{t}$. To address this problem, we exploit the above obtained results regarding computation of the next-state probabilities, $p(q_{t+1}=j|\{\boldsymbol{o}_\tau\}_{\tau=1}^{t})$. Specifically, we effect the sequence prediction task at time $t+1$ as follows:
(i) We use Eq. (38) to obtain the emitting state probabilities at the following time point $(t+1)$, given the current set of observations (up to time t), i.e. $p(q_{t+1}=j|\{\boldsymbol{o}_\tau\}_{\tau=1}^{t})$.
(ii) We set the generated predicted value $\hat{\boldsymbol{o}}_{t+1}$ of the observation at time $t+1$ equal to the mean value of the modeled variable $\boldsymbol{o}$ at time $t+1$, based on the fitted VDJ-HMM model with parameters set $\hat{\Theta}$. Specifically, considering mixtures of Gaussians or Student's-t densities as the emission distributions of our model, as discussed previously, this procedure yields:

$$\hat{\boldsymbol{o}}_{t+1} = \sum_{n=1}^{N}\sum_{m=1}^{M} p(q_{t+1}=n|\{\boldsymbol{o}_\tau\}_{\tau=1}^{t}) w_{nm}\boldsymbol{\mu}_{nm} \tag{40}$$

E. Computational Complexity

We conclude this section with a short discussion on the computational complexity of our model. From Eqs. (19)-(27), we can easily observe that the main difference between VDJ-HMM and a simple first-order HMM concerns computation of the set of forward and backward probabilities, $\{\alpha_t(j,k)\}_{t,j,k}$ and $\{\beta_t(j,k)\}_{t,j,k}$, respectively, which are distinct for each possible temporal dependence pattern, $k=1,\ldots,K$. Indeed, the computational complexity of computing the forward and backward probabilities of a first-order HMM comprising N states and M component Gaussian distributions per state, given a D-dimensional observed sequence of length T, can be shown to be $\mathcal{O}(3N^2T + NTMD)$. Consequently, the corresponding computational complexity in the case of our model becomes $\mathcal{O}(3N^2TK + NTMDK)$, where K is the maximum order of the postulated model. Hence, the related increase in computational complexity introduced by our model is linear w.r.t. K.

III. Experiments

In this section, we perform an extensive evaluation of the proposed VDJ-HMM model. For this purpose, we first consider a set of time-series forecasting experiments dealing with real-world applications from the computational finance domain. Further, we consider a computer vision application,

Table II: EUR-USD exchange rate volatility: Performance (RMSE) of the evaluated methods.

	HMM (Gaussian)	HMM (Student's-t)	Second Order HMM (Gaussian)	Third Order HMM (Gaussian)	HMM$^{\infty}$ (Gaussian)	HMM$^{\infty}$ (Student's-t)
3/3/2009 - 10/12/2009	1.607	1.559	1.599	1.593	1.591	1.534
10/13/2009 - 5/25/2010	0.738	0.721	0.734	0.730	0.730	0.713
5/26/2010 - 12/30/2010	0.683	0.696	0.681	0.680	0.677	0.691
Total	1.094	1.07	1.090	1.087	1.086	1.059

Table III: EUR-USD exchange rate volatility: Performance (RMSE) of the evaluated methods (cont.).

	HSMM (Geometric - Gaussian)	HSMM (Geometric - Student's-t)	VDJ-HMM (Gaussian)	VDJ-HMM (Student's-t)
3/3/2009 - 10/12/2009	1.689	1.74	1.504	1.435
10/13/2009 - 5/25/2010	0.717	0.703	0.7	0.702
5/26/2010 - 12/30/2010	0.681	0.687	0.672	0.669
Total	1.113	1.146	1.028	1.011

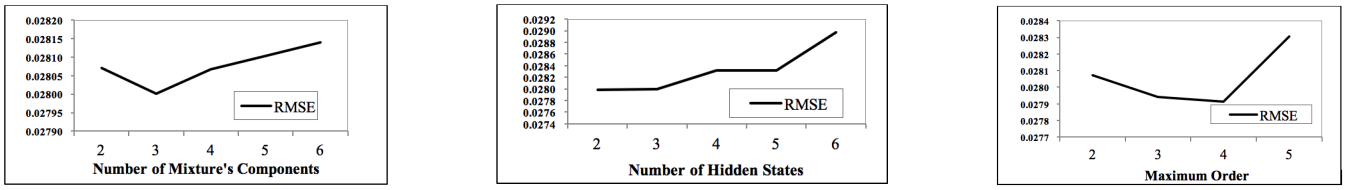

(a) (b) (c)

Figure 2: EUR-USD exchange rate volatility: Performance (RMSE) fluctuation obtained by varying model configuration (validation set).

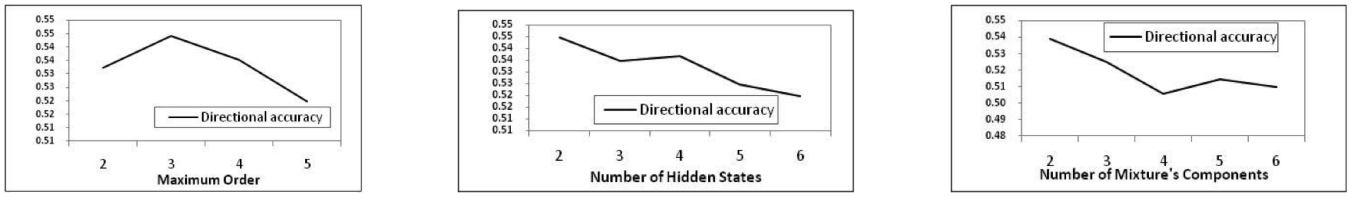

(a) (b) (c)

Figure 3: EUR-USD exchange rate price prediction: Performance fluctuation (directional prediction accuracy) obtained by varying model configuration (validation set).

Table IV: Time-series of multiple correlated exchange rates and market indices: Optimal VDJ-HMM model configuration under the univariate modeling setup.

Parameter	Value
K	3
N	2
M	2

dealing with the problem of visual workflow recognition from sequences of depth images.

Specifically, we begin by considering *volatility forecasting* and *return value prediction* in financial return series. Broad empirical evidence (see, e.g. [18], [20], [22]) has shown that financial return series exhibit variable order non-linear temporal dependencies, as well as dependence jumps, both when it comes to *volatility forecasting* and concerning *future value prediction*. As such, leveraging the merits of our model in the context of these applications is expected to yield a significant performance improvement over the competition. To provide some comparative results, apart from our method we also evaluate the related HMM$^{\infty}$ model [12], which postulates infinitely-long temporal dependencies at each time point, baseline first-order, second-order, and third-order HMMs, and explicit-duration HSMMs [29]. In addition, we cite the performance of other popular alternatives, as they have been reported in the recent literature.

At this point, we must underline that the order of asset price return series is typically *up to* two, while for asset volatility it is usually *up to* three (see, e.g. [19]). Hence, one can expect that the values of K discovered by VDJ-HMM should not normally exceed that level. This fact, in turn, strongly implies that any observed performance differences between

Table V: Time-series of multiple correlated exchange rates and market indices: Performance (RMSE) obtained under the univariate modeling setup.

Scenario	HMM	Second Order HMM	Third Order HMM	HSMM	HMM$^{\infty}$	GARCH	VHGP	GPMCH	VDJ-HMM
#1	0.0442	0.0303	0.0250	0.0292	0.0235	0.0705	0.0146	0.0121	0.0108
#2	0.0841	0.0419	0.0357	0.0589	0.0353	0.2785	0.0552	0.0360	0.0351
#3	0.0744	0.0455	0.0334	0.0578	0.0331	0.0552	0.0542	0.0345	0.0329

Table VI: Time-series of multiple correlated exchange rates and market indices: Optimal VDJ-HMM model configuration under the multivariate modeling setup.

Parameter	Value
K	3
N	2
M	2

our approach and medium-order HMMs should be due to the *variable-order modeling* capabilities of our approach, rather than the adopted (maximum) model order *per se.* In all cases, to ensure the validity of our comparisons, we perform model training following *exactly the same experimental setup* as in the case of the cited papers.

Finally, our evaluations dealing with computer vision applications are performed using a publicly available database, while performance comparisons are made against some popular alternatives, including hidden conditional random fields (H-CRFs) [30], dual-functionality conditional random fields (DF-CRFs) [31], as well as baseline first-order, second-order, and third-order HMMs.

A. Financial Time-Series Modeling

1) Volatility Forecasting: In this set of experiments, we apply our model to prediction of the volatility in daily returns of financial assets. Consider a modeled asset with price P_t at time t; then, its daily return at time t is defined as the logarithm $r_t \triangleq \log \frac{P_t}{P_{t-1}}$. On this basis, (historic) volatility is defined as the square of the return series r_t^2; as discussed in [32], this groundtruth measurement constitutes one of the few consistent ways of volatility measuring. To evaluate the considered algorithms, we employ performance metrics typically considered in the literature. These include the root mean squared error (RMSE) between the model-estimated volatilities and the squared returns of the modeled return series, the corresponding mean square error (MSE), or the corresponding mean absolute error (MAE).

In all cases, our experimental setup is the following: For each one of the considered applications, we split the available data into a training sample, a validation sample, and a testing sample; we adopt the same splits as the authors of the state-of-the-art methods reported in the literature, to render our performance measurements comparable with these results. We use the available training samples to train multiple VDJ-HMM models with different configurations; specifically, we evaluate models with different maximum allowed numbers of alternative temporal dependence patterns (maximum steps back) K, numbers of emitting states N, and numbers of mixture components per emitting state M. We select the optimal model configuration on the basis of the obtained predictive performances on the available validation samples. Finally, we use the available test samples to obtain the reported performance figures. Similar is the experimental setup we adopt for the considered competitors. In all cases, to alleviate the effect of random model initialization on the reported performance results, we repeat our experiments 10 times, with different model initializations each time, and report average performance figures over these repetitions.

Euro-United States Dollar exchange rate volatility: Our first experimental scenario regarding volatility forecasting is dealing with the EUR-USD exchange rate time series[1]. Specifically, for the purposes of this experiment, we use data from the period 5/17/2007 – 8/10/2008 as our training set, and data pertaining to the period 9/10/2008 - 2/3/2009 as our validation set. To perform model evaluation, we consider three distinct test samples, pertaining to the periods: 3/3/2009 - 10/12/2009, 10/13/2009 - 5/25/2010, and 5/26/2010 - 12/30/2010, respectively. This way, we allow for evaluating model performance in periods with different levels of inherent volatility in the European economy. In all cases, the evaluated methods are trained using a rolling window of the previous 60 days of returns to make daily volatility forecasts for the following 10 days. Under this setup, we essentially retrain the models every 10 days, allowing for adapting to *structural breaks* in the EUR-USD exchange rate time series that cannot be accounted for otherwise. We use both Gaussian mixtures and Student's-t mixtures as the state-conditional emission distributions. In the case of the HSMM method, we consider Poisson, Negative Binomial, Geometric, and Logarithmic densities for modeling state duration.

In Table I, we depict the optimal configuration parameters of our model, obtained by utilizing the available validation set, as described previously. In Tables II and III, we illustrate the obtained performances of the evaluated methods. Note that these results are obtained for optimal model configuration (as determined in the validation set) both in the case of our model and the considered competitors. As we observe, in all cases our VDJ-HMM model yields the best performance among the evaluated methods. In addition, it appears that utilization of Student's-t mixture emission distributions yields in most cases only negligible performance improvements over models postulating Gaussian mixture emission distributions. We also observe that the HSMM model yielded best performance when postulating Geometric state duration distributions (we omit the results pertaining to different HSMM model configurations for brevity).

[1]The used data have been obtained from the official website of the European Central Bank.

Table VII: Time-series of multiple correlated exchange rates and market indices: Performance (RMSE) obtained under the multivariate modeling setup.

	HMM	Second Order HMM	Third Order HMM	HMM$^{\infty}$	GPMCH	VDJ-HMM
Scenario #1	0.0345	0.0338	0.0335	0.0333	0.0341	0.0330
Scenario #2	0.0712	0.0682	0.0614	0.0609	0.0557	0.0605
Scenario #3	0.1512	0.1416	0.1212	0.1109	0.9905	0.0744

Table VIII: Oil price time-series volatility: Optimal VDJ-HMM model configuration.

Parameter	Value: Brent	Value: WTI
K	3	3
N	2	2
M	3	4

Table IX: Oil price time-series volatility: Performance (MSE and MAE) of the evaluated approaches.

Method	Brent (MSE)	Brent (MAE)	WTI (MSE)	WTI (MAE)
GARCH	0.698	0.065	0.933	0.693
IGARCH	0.856	0.000	0.690	0.000
GJR	0.987	0.811	0.847	0.000
EGARCH	0.609	0.000	0.058	0.000
APARCH	0.557	0.002	0.846	0.031
FIGARCH	0.083	0.111	0.514	0.074
FIAPARCH	0.157	0.586	0.501	0.668
HYGARCH	0.080	0.030	0.546	0.000
HMM	0.087	0.095	0.200	0.067
2-Order HMM	0.082	0.091	0.194	0.071
3-Order HMM	0.080	0.088	0.192	0.070
HSMM	0.100	0.090	0.181	0.090
HMM$^{\infty}$	0.079	0.088	0.191	0.071
VDJ-HMM	0.050	0.001	0.044	0.000

Finally, in Figs. 2a-2c, we illustrate how model performance changes by varying model configuration, i.e. the hyperparameter values K (maximum order of dependence jumps), N (number of emitting states), and M (number of mixture components). Specifically, in each one of these figures we show how performance changes by altering the values of one hyperparameter in the set $\{K, N, M\}$, while keeping the other two equal to their determined best value. It is apparent that model configuration plays a critical role in the obtained performance. This is especially true for the maximum order of dependence jumps K: selecting too big a value results in performance deterioration, while values close to $K = 1$ (i.e., reducing to a simple first-order HMM) yield inferior performance compared to a fully-fledged VDJ-HMM.

Table X: Gold market time-series volatility: Optimal VDJ-HMM model configuration.

Parameter	Value
K	3
N	3
M	2

Time-series of multiple correlated exchange rates and market indices: In this set of experiments, we consider three application scenarios:

- In the first scenario, we model the return series pertaining to the following *currency exchange rates,* over the period December 31, 1979 to December 31, 1998 (daily closing prices):
  1. (AUD) Australian Dollar / US $
  2. (GBP) UK Pound / US $
  3. (CAD) Canadian Dollar / US $
  4. (DKK) Danish Krone / US $
  5. (FRF) French Franc / US $
  6. (DEM) German Mark / US $
  7. (JPY) Japanese Yen / US $
  8. (CHF) Swiss Franc / US $.
- In the second scenario, we model the return series pertaining to the following *global indices,* for the business days over the period April 27, 1993 to July 14, 2003 (daily closing prices):
  1. (TSX) Canadian TSX Composite
  2. (CAC) French CAC 40
  3. (DAX) German DAX
  4. (NIK) Japanese Nikkei 225
  5. (FTSE) UK FTSE 100
  6. (SP) US S&P 500.
- Finally, in the third scenario, we model the return series pertaining to the following seven indices, for the business days over the period February 7, 2001 to April 24, 2006 (daily closing prices for the first 6 indices, and annual percentage rate converted to daily effective yield for the last index):
  1. (TSX) Canadian TSX Composite
  2. (CAC) French CAC 40
  3. (DAX) German DAX
  4. (NIK) Japanese Nikkei 225
  5. (FTSE) UK FTSE 100
  6. (SP) US S&P 500
  7. (EB3M) Three-month Euribor rate.

These series have become standard benchmarks for assessing the performance of volatility prediction algorithms [33], [34], [35]. In our experiments, we follow an evaluation protocol similar to [34], [36]. We adopt the same data split as in [36]; all the evaluated methods are trained using a rolling window of the previous 120 days of returns to make daily volatility forecasts for the following 10 days. Under this setup, we essentially retrain the models every 7 days, allowing for adapting to *structural breaks* in the markets, similar to the

Table XI: Gold market time-series volatility: Performance (MSE and MAE) of the evaluated approaches.

	HM	MA(20)	MA(40)	MA(120)	HMM	HSMM	Second Order HMM	Third Order HMM	HMM$^\infty$
MSE	105.24	84.64	83.29	87.97	85.77	85.5	84.89	84.56	84.52
MAE	5.43	5.96	5.72	5.40	5.69	5.82	5.67	5.63	5.63

Table XII: Gold market time-series volatility: Performance (MSE and MAE) of the evaluated approaches (cont.).

	AR(5)	MAD(5)	ARMA	EMWA	GARCH	GARCH-M	VDJ-HMM
MSE	86.08	90.08	84.24	83.81	86.94	86.35	84.16
MAE	5.67	5.54	5.68	5.84	5.56	5.68	5.60

Table XIII: EUR-USD exchange rate price prediction: Optimal VDJ-HMM model configuration.

Parameter	Value
K	3
N	2
M	2

Table XIV: EUR-USD exchange rate price prediction: Performance of the evaluated models.

Model	Directional Accuracy	Annualized Return
KNN	50.11	-2.26
Naïve Bayes	48.83	-3.08
BP	50.12	1.59
SVM	52.65	3.98
RF	53.50	7.28
HMM	52.5	4.05
2-Order HMM	52.9	5.13
3-Order HMM	53.17	6.6
HSMM	51.2	1.5
HMM$^\infty$	53.18	6.44
VDJ-HMM	54.05	9.50

previous experiment.

To begin with, we consider modeling each asset with a different VDJ-HMM model; i.e. we postulate as many VDJ-HMM models as the assets modeled in each scenario. The same *univariate* setup is also adopted for the considered HMM-based competitors[2]. Under this setup, the determined optimal configuration for our model is provided in Table IV. In Table V, we provide the obtained results for the three considered scenarios (for optimal model configuration, as determined in the validation set). These results are computed over all the assets modeled in each scenario (averages). The performances of the state-of-the-art methods GARCH [37], [38], VHGP [39], and GPMCH [36] have been cited from [36]. We observe that VDJ-HMM performs better than the competition in all scenarios, with the obtained performance differences becoming more significant in the case of scenario #1, which involves *only* currency exchange rates in the set of modeled assets. We tend to attribute this finding to the fact that currency exchange rates have a unique *mean-reverting property* [40], which seems that our proposed VDJ-HMM model is capable of capturing much better than the competition.

Further, we consider the case of jointly modeling all the assets available in each scenario. For this purpose, we essentially postulate VDJ-HMM models with D-variate emission distributions, where D is the number of jointly modeled assets. The same holds for all the considered HMM-type competitors of our method. In Table VI, we report the determined optimal configuration of our model for this experimental setup. The corresponding predictive performances are reported in Table VII. In this table, we also cite the performance of the multi-output GPMCH model (using Clayton copulas), as reported in [36]. As we observe, our approach yields results comparable to or slightly better than the state-of-the-art in all cases. Note also that this performance improvement does also come for a significantly lower computational complexity compared to the second best performing method in these experiments, i.e. the GPMCH method (which, for instance, entails expensive computation and inversion of large gram matrices).

Oil price time-series volatility: Further, we consider the problem of volatility forecasting in oil prices. For this purpose, and similar to the experimental setup of [41], we use the daily price data of the Brent index and the West Texas Intermediate (WTI) index from January 6, 1992, to December 31, 2009 (prices expressed in US dollars per barrel). From these time-series, the data pertaining to the last three years, i.e., 2007 to 2009, are used to evaluate the predictive performance of the evaluated models, while the data pertaining to the period 1/3/2006 - 12/29/2006 are used as our validation sample (and the rest for model training). All the evaluated methods are trained using a rolling window of the previous 60 days of returns to make daily volatility forecasts; we retrain the models every 5 days.

In Table VIII, we report the optimal configuration of our model for our experiments with both time-series (Brent and WTI). In Table IX, we provide the obtained performances of the evaluated models. Note that all HMM-based models are evaluated using Gaussian mixture emission distributions. The performances of ARCH and its variants have been reported from [41]. As we observe, the proposed VDJ-HMM model consistently yields the best observed performance expressed in terms of the resulting MSE metric, with significant performance differences from all the considered competitors. On the other hand, when evaluation is performed using the MAE metric, we observe that our method manages to yield performance

[2]All HMM-based models are evaluated using Gaussian mixture emission distributions.

Table XV: Action recognition from depth images: Confusion matrix for the segmentation task. The results are normalized based on the total number of frames per activity, considering all cross-validation runs.

		Recognized Class	
		1	2
True Class	1	.69	.31
	2	.16	.84
Total error = 23.34%			

(a) HMM

		Recognized Class	
		1	2
True Class	1	.74	.26
	2	.13	.87
Total error = 17.45%			

(b) Second-Order HMM

		Recognized Class	
		1	2
True Class	1	.77	.23
	2	.12	.88
Total error = 16.86%			

(c) Third-Order HMM

		Recognized Class	
		1	2
True Class	1	.836	.163
	2	.107	.893
Total error = 13.50%			

(d) CRF

		Recognized Class	
		1	2
True Class	1	.925	.075
	2	.09	.91
Total error = 8.25%			

(e) DF-CRF

		Recognized Class	
		1	2
True Class	1	.97	.03
	2	.034	.966
Total error = 2.91%			

(f) VDJ-HMM

comparable to the state-of-the-art, but it cannot obtain further improvements; note though that the reported state-of-the-art MAEs are already exceptionally low, and therefore the room for further performance improvement is rather limited.

Gold market time-series volatility: Here, we explore the performance of VDJ-HMM in volatility prediction for daily return series of Gold. The dataset used for this experiment consists of the daily Gold fixing prices of the London Bullion Market[3]. Specifically, following [42], we use the daily PM fixings price released at 15:00, and forecast the daily volatility during the second semester of 2008. This is an interesting and quite challenging experimental scenario, since the considered forecast period coincides with the period when the recent financial crisis took place. Similar to [42], our training and validation samples pertain to the period 1/4/1999 - 6/30/2008, while evaluation is performed using the MSE and MAE metrics.

In Table X, we report the optimal configuration of our model. In Tables XI-XII, we provide the obtained performances of the evaluated models. Note that all HMM-based models are evaluated using Gaussian mixture emission distributions. The performances of the reported state-of-the-art competitors, namely historical mean (HM), autoregressive models (AR(k)), moving average models (MA(k) and EWMA), ARMA, as well as several GARCH variants [38], [37], have been cited from [42]. As we observe, the proposed VDJ-HMM model yields a quite satisfactory performance in this experiment, yielding error figures comparable to the state-of-the-art results reported in the recent literature.

2) Return Value Prediction: Finally, we apply our model to prediction of the future values of the daily return series of modeled financial assets, r_t. Specifically, under our experimental setup, we are interested in correctly predicting the sign of the return value at future time points. This sign can be used as the foundation of a simple portfolio management policy as follows: If the predicted future return sign is positive, then the policy suggests that the asset be retained by the investment portfolio manager; on the other hand, if the predicted future return sign is negative, then the policy creates a "sell" signal. All HMM-based models evaluated in these experiments postulate Gaussian mixture models as their emission distributions.

To this end, we consider the task of future value prediction for the EUR-USD exchange rate. We use a training sample pertaining to the period 1/17//2002 – 5/16/2008, a validation sample pertaining to the period 5/17/2008 - 3/2/2009, and a test sample pertaining to the period 3/3/2009 - 12/30/2010. All the evaluated methods are trained using a rolling window of the previous 60 days of returns to make daily price prediction for the following 10 days; we retrain the models every 5 days.

On this basis, model evaluation is performed according to: (i) the comparison of the signs of the generated predictions with the actual ones (hereafter referred to as *directional prediction*); and (ii) the resulting annualized return of the aforementioned portfolio management policy, defined as the mean obtained profit adjusted for the return standard deviation over the whole forecasting period.

In Table XIII, we depict the optimal configuration of our VDJ-HMM model as determined by utilizing the available validation set. In Figs. 3a-3c, we show how VDJ-HMM model performance changes by varying the adopted configuration (results obtained on the available validation set). As we observe, model configuration plays a crucial role to the obtained performance. Further, another interesting finding is that, similar to the volatility forecasting experiment, model performance reaches its optimal value for a moderate value of K, while experiencing a significant decrease for too high values of K or when $K = 1$.

In Table XIV, we provide the obtained performance results for the evaluated methods (for optimal model configuration). Note that the performances of the methods k-nearest neighbor (KNN), Naïve Bayes, back-propagation neural network (BP), support vector machine (SVM) [43], and random forest (RF) [44] have been cited from [45]. As we observe, our method completely outperforms the competition, yielding the state-of-the-art result in this dataset.

[3]Data obtained from the official website of the London Bullion Market Association (www.lbma.org.uk).

B. Action recognition from depth images

In these experiments, we apply our method to data dealing with a computer vision application. Specifically, we consider the task of classifying sequences of depth images, which depict humans performing actions in an assistive living environment. To this end, we use the dataset described in [46], which includes several actions from which we have selected the following: (1) get up from bed, (2) go to bed, (3) sit down, (4) eat meal, and (5) drink water. We seek to recognize two activities: activity #1 comprises actions (1)-(2) (see Fig. 4 for an example); activity #2 comprises actions (3),(4),(5). In all cases, the observable input is the sequence of vectors $\boldsymbol{x}$, which is extracted as described next. Due to the aforementioned nature of the modeled dataset, we expect that this experiment will allow us to: (i) exhibit the applicability of our approach to data from diverse application domains; and (ii) evaluate our method in a setting where quite high maximum order values might be needed in order to successfully model the observed data (contrary to financial data modeling, where maximum order values are not theoretically expected to exceed $K = 3$, as we confirmed in the majority of our previous experiments).

For each depth image, we extract features similar to [46] using a variation of Motion History Images (MHIs). MHIs are among the first holistic representation methods for behavior recognition [47]. In an MHI H_τ, pixel intensity is a function of the temporal history of motion at that point.

$$H_\tau^I(x,y,t) = \begin{cases} \tau, \text{if } |I(x,y,t) - I(x,y,t-1)| > \delta I_{th} \\ max(0, H_\tau^I(x,y,t-1) - 1), \text{otherwise.} \end{cases} \tag{41}$$

Here, τ is the longest time window we want the system to consider, and δI_{th} is the threshold value for generating the mask for the region of motion. The result is a scalar-valued image where more recently moving pixels are brighter. Note that the MEI can be generated by thresholding the MHI above zero. Ni et al. [46] proposed the use of a depth sensor, and introduced the motion history along the depth changing directions. To encode the backward motion history (decrease of depth), they introduced the backward-DMHI (bDMHI):

$$H_\tau^{fD}(x,y,t) = \begin{cases} \tau, \text{if } D(x,y,t) - D(x,y,t-1) < -\delta I_{th} \\ max(0, H_\tau^{fD}(x,y,t-1) - 1), \text{otherwise.} \end{cases} \tag{42}$$

Here, H_t^{bD} denotes the backward motion history image and $D(x,y,t)$ denotes the depth sequence. δI_{th} is the threshold value for generating the mask for the region of backward motion. Similarly is defined the forward history image, which we don't use in our experiments, but is expected to give similar results.

In order to calculate the depth change-induced motion history images, according to the above equations, we use depth maps captured by a Kinect™ device. However, Kinect depth maps have the main disadvantage of the presence of a significant amount of noise. After frame differencing and thresholding, we noticed that motion is encoded even in areas where there are only still objects. To tackle this problem, we use a median filtering at the spatial domain. In the temporal domain, each pixel value is replaced by the minimum of its neighbors. The MHI images are represented by means of the complex Zernike coefficients A_{00}, A_{11}, A_{20}, A_{22}, A_{31}, A_{33}, A_{40}, A_{42}, A_{44}, A_{51}, A_{53}, A_{55}, A_{60}, A_{62}, A_{64}, A_{66}, for each of which the norm and the angle are included in the provided descriptors. We use a total of 31 parameters (constant elements were removed), thus providing an acceptable scene reconstruction without a computationally prohibitive dimension.

In our experiments, we use 35 action sets per type (these are the first 35 samples in the dataset for each action). We use cross-validation in the following fashion: in each cycle, fifteen of these sets are randomly selected to perform training, and the rest twenty are used for testing. We run the same experiment 50 times to account for the effect of random selection of samples. To evaluate the sequence classification performance of our model, we use our model to classify the test workflows into two classes corresponding to actions 1 and 2, respectively. For comparison, we repeat the same experiment using baseline first-order, second-order, and third-order HMMs, HCRFs with 4 hidden states, and the DF-CRF method, trained as described in [30] and [31], respectively.

The obtained results are given in Table XV; therein, the reported "optimal" performance of VDJ-HMM has been obtained with $M = 3, N = 2, K = 8$. As we observe, our approach outperforms the competition, including the popular HCRF method, and the recently proposed DF-CRF approach. We also underline here that, in order to examine the statistical significance of the reported differences between the evaluated methods, we have made use of the Student-t hypothesis test; our results have verified the statistical significance of the observed performance differences, in all cases. Finally, it is interesting to emphasize that the best performance of VDJ-HMM is obtained with the maximum model order set to $K = 8$. Since the used dataset is well-expected to entail long temporal dynamics (contrary to the previously considered financial time-series, where high K values are not expected to be needed due to frequent changes in the economic cycles), this finding supports our claims regarding the capability of our approach to capture the actual (variable) length of the temporal dynamics entailed in the modeled data.

C. Further Examination

We conclude the experimental section of our work, attempting to get a better feeling of whether our model actually captures *variable* forms of temporal dependencies, and how often related dependence jumps actually take place. To this end, we focus on one example use case of Section III.A, namely gold market time-series volatility prediction. In Fig. 5, we show the obtained values of the posterior probabilities $\zeta_{kt} \triangleq E(z_t = k|O)$ at each time point, where $k \in \{1,2,3\}$. As we observe, the possibility $z_t = 1$ takes the highest posterior probability most often, followed by the possibility $z_t = 3$, while $z_t = 2$ yields the highest posterior probability value least often. In an attempt to explain these findings, in Fig. 6 we show how the value of z_t yielding the maximum posterior probability fluctuates with the corresponding (historic) volatility values. We observe that high volatility periods

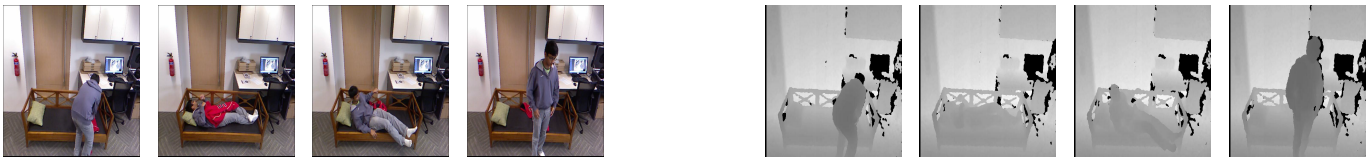

(a) Color images (b) Depth images

Figure 4: Key frames from activity 1: action 1 - go to bed (frames 1,2), and action 2 - get up from bed (frames 3,4))

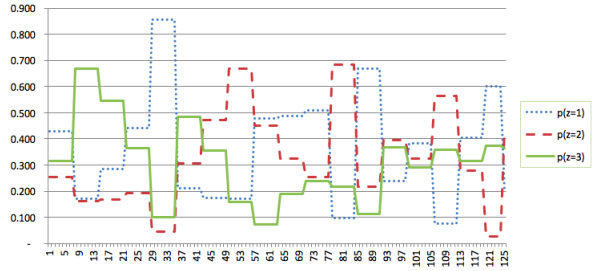

Figure 5: Gold market time-series volatility: $p(z_t|O)$ values at each time point.

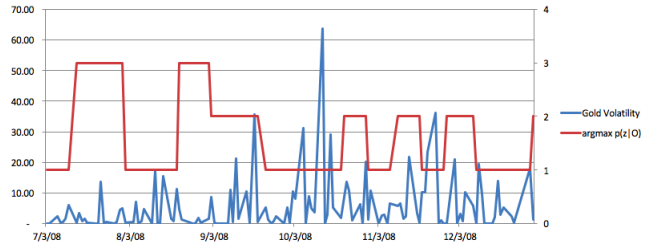

Figure 6: Gold market time-series volatility: $\hat{z}_t = \text{argmax}p(z_t|O)$ values fluctuation with historic volatility.

result in the winning values of z_t being equal to *one* (or *two* in some rare occasions), while low volatility periods may result in winning values of z_t equal to *three*. In our view, this is a quite interesting and encouraging finding: Indeed, high volatility periods are characterized by structural breaks that render assumptions of long temporal dependencies rather invalid. On the contrary, such assumptions may be accurate and useful for the modeling algorithm when volatility is low.

IV. Conclusions

In this paper, we focused on the problem of modeling sequential data the temporal dynamics of which may switch between different patterns over time. To address this problem, we introduced a hierarchical model comprising two hidden chains of temporal dependencies: on the *first layer*, our model comprises a *chain* of *latent observation-emitting states,* the *dependencies* between which may *change over time*; on the *second layer,* our model utilizes a *latent first-order Markov chain* modeling the *evolution* of temporal dynamics pertaining to the first-layer latent process. To allow for tractable training and inference procedures, our model considers *temporal dependencies* taking the form of *variable order dependence jumps*, the order of which is *inferred* from the data as part of the model inference procedure. We devised efficient model training and inference algorithms under the maximum-likelihood paradigm.

To evaluate the capacity of our method in effectively modeling non-homogeneous observed sequential data, where the patterns of temporal dependencies may change over time, we considered a number of applications from diverse domains. Our experimental results provided strong evidence that our method is actually capable of delivering on its goals. As we showed, these encouraging performance results come for only an increase in computational complexity linear w.r.t. K compared to baseline first-order HMMs. Taking into consideration that the maximum required K value in our real-world application experiments did not exceed $K = 9$, we can, thus, argue that our method offers a favorable performance/complexity trade-off.

An issue we have not fully addressed in this work is how we could allow for automatic determination of the optimal model configuration, without the need of resorting to cross-validation (as we did in our experimental evaluations). For this purpose, one could resort to devising a nonparametric Bayesian construction for the VDJ-HMM model, by imposing appropriate priors over the model parameters (e.g., Dirichlet process priors [48] over the transition probability matrices of our model), and performing Bayesian inference instead of maximum-likelihood training. This issue remains to be addressed in our future work.

References

[1] O. Cappé, E. Moulines, and T. Rydén, *Inference in Hidden Markov Models*. New York: Springer Series in Statistics, 2005.

[2] J. Mari, D. Fohr, and J. Junqua, "A second-order HMM for high-performance word and phoneme-based continuous speech recognition," in *Proc. of the IEEE International Conference on Acoustics, Speech and Signal Processing*, 1996, pp. 435–438.

[3] J.-F. Mari, J.-P. Haton, and A. Kriouile, "Automatic word recognition based on second-order hidden Markov models," *IEEE Trans. Speech Audio Process.*, vol. 5, no. 3, pp. 22–25, 1997.

[4] E.-M. Nel, J. D. Preez, and B. Herbst, "Estimating the pen trajectories of static signatures using hidden Markov models," *IEEE Trans. Pattern Anal. Mach. Intell.*, vol. 27, no. 11, pp. 1733–1746, 2005.

[5] C. Eng, A. Thibessard, S. Hergalant, J.-F. Mari, and P. Leblond, "Data mining using hidden Markov models (HMM2) to detect heterogeneities into bacteria genomes," in *Journes Ouvertes Biol. Inf. Math. (JOBIM)*, 2005.

[6] O. Aycard, J.-F. Mari, and R. Washington, "Learning to automatically detect features for mobile robots using second-order hidden Markov models," *Int. J. Adv. Robotic Syst.*, vol. 1, no. 4, pp. 231–245, 2004.

[7] H. Engelbrecht and J. du Preez, "Efficient backward decoding of high-order hidden Markov models," *Pattern Recognition*, vol. 43, no. 1, pp. 99–112, 2010.

[8] G. McLachlan and D. Peel, *Finite Mixture Models*. Wiley Series in Probability and Statistics, 2000.

[9] S. P. Chatzis, "Margin-maximizing classification of sequential data with infinitely-long temporal dependencies," *Expert Systems with Applications*, vol. 40, no. 11, pp. 4519–4527, 2013.

[10] R. Begleiter, R. El-Yaniv, and G. Yona, "On prediction using variable order Markov models," *Journal of Machine Learning Research*, vol. 22, pp. 385–421, 2004.

[11] C. Dimitrakakis, "Bayesian variable order Markov models," in *Proc. AISTATS*, 2010, pp. 161–168.

[12] S. P. Chatzis, D. I. Kosmopoulos, and G. M. Papadourakis, "A nonstationary hidden Markov model with approximately infinitely-long time-dependencies," in *Proc. ISVC*, vol. 2, 2014, pp. 51–62.

[13] P. Bühlmann and A. J. Wyner, "Variable length markov chains," *Ann. Statist.*, vol. 27, no. 2, pp. 480–513, 04 1999.

[14] F. Chierichetti, R. Kumar, P. Raghavan, and T. Sarlos, "Are web users really markovian?" in *Proceedings of the 21st International Conference on World Wide Web*, ser. WWW '12. New York, NY, USA: ACM, 2012, pp. 609–618.

[15] M. J. Zaki, C. D. Carothers, and B. K. Szymanski, "VOGUE: A Variable Order Hidden Markov Model with Duration based on Frequent Sequence Mining," *ACM Transactions on Knowledge Discovery from Data*, vol. 4, no. 1, pp. 1–31, 2010.

[16] A. Dempster, N. Laird, and D. Rubin, "Maximum likelihood from incomplete data via the EM algorithm," *Journal of the Royal Statistical Society, B*, vol. 39, no. 1, pp. 1–38, 1977.

[17] C. Stărică and C. Granger, "Nonstationarities in stock returns," *Review of economics and statistics*, vol. 87, no. 3, pp. 503–522, 2005.

[18] S. J. Taylor, *Modelling financial time series*. World Scientific Publishing Company, 2007.

[19] R. Cont, "Empirical properties of asset returns: stylized facts and statistical issues," *Quantitative Finance*, vol. 1, pp. 223–236, 2001.

[20] Z. Ding, C. W. Granger, and R. F. Engle, "A long memory property of stock market returns and a new model," *Journal of empirical finance*, vol. 1, no. 1, pp. 83–106, 1993.

[21] V. Todorov and G. Tauchen, "Volatility jumps," *Journal of Business & Economic Statistics*, vol. 29, no. 3, pp. 356–371, 2011.

[22] B. Eraker, "Do stock prices and volatility jump? Reconciling evidence from spot and option prices," *The Journal of Finance*, vol. 59, no. 3, pp. 1367–1404, 2004.

[23] B. Eraker, M. Johannes, and N. Polson, "The impact of jumps in volatility and returns," *The Journal of Finance*, vol. 58, no. 3, pp. 1269–1300, 2003.

[24] T. Rydén, T. Teräsvirta, and S. Åsbrink, "Stylized facts of daily return series and the hidden Markov model," *Journal of applied econometrics*, vol. 13, no. 3, pp. 217–244, 1998.

[25] J. Bulla and I. Bulla, "Stylized facts of financial time series and hidden semi-Markov models," *Computational Statistics & Data Analysis*, vol. 51, no. 4, pp. 2192–2209, 2006.

[26] A. Petropoulos, S. P. Chatzis, and S. Xanthopoulos, "A novel corporate credit rating system based on student's-t hidden markov models," *Expert Systems with Applications*, vol. 53, pp. 87–105, 2016.

[27] S. P. Chatzis, D. I. Kosmopoulos, and T. A. Varvarigou, "Robust sequential data modeling using an outlier tolerant hidden Markov model," *IEEE Transactions on Pattern Analysis and Machine Intelligence*, vol. 31, no. 9, pp. 1657–1669, 2009.

[28] L. Rabiner, "A tutorial on hidden Markov models and selected applications in speech recognition," *Proceedings of the IEEE*, vol. 77, pp. 245–255, 1989.

[29] S. Yu, "Hidden semi-Markov models," *Artificial Intelligence*, vol. 174, no. 2, pp. 215–243, 2010.

[30] A. Quattoni, S. Wang, L.-P. Morency, M. Collins, and T. Darrell, "Hidden conditional random fields," *IEEE Trans. Pattern Anal. Mach. Intell.*, vol. 29, no. 10, pp. 1848–1853, 2007.

[31] S. P. Chatzis, D. Kosmopoulos, and P. Doliotis, "A conditional random field-based model for joint sequence segmentation and classification," *Pattern Recognition*, vol. 46, no. 6, pp. 1569–1578, 2013.

[32] C. T. Brownlees, R. F. Engle, and B. T. Kelly, "A practical guide to volatility forecasting through calm and storm," 2009, available at SSRN: http://ssrn.com/abstract=1502915.

[33] B. McCullough and C. Renfro, "Benchmarks and software standards: A case study of GARCH procedures," *Journal of Economic and Social Measurement*, vol. 25, pp. 59–71, 1998.

[34] A. G. Wilson and Z. Ghahramani, "Copula processes," in *Advances in Neural Information Processing Systems*, 2010.

[35] C. Brooks, S. Burke, and G. Persand, "Benchmarks and the accuracy of GARCH model estimation," *International Journal of Forecasting*, vol. 17, pp. 45–56, 2001.

[36] E. A. Platanios and S. P. Chatzis, "Gaussian process-mixture conditional heteroscedasticity," *IEEE Trans. Pattern Anal. Mach. Intell.*, vol. 36, no. 5, pp. 888–900, May 2014.

[37] T. Bollerslev, "Generalized autoregressive conditional heteroskedasticity," *Journal of Econometrics*, vol. 94, pp. 238–276, 1986.

[38] R. Engle, "Autoregressive conditional heteroskedasticity models with estimation of variance of United Kingdom inflation," *Econometrica*, vol. 50, pp. 987–1007, 1982.

[39] M. Lázaro-Gredilla and M. Tsitsias, "Variational heteroscedastic Gaussian process regression," in *Proc. 28th International Conference on Machine Learning*, Bellevue, WA, USA, 2011.

[40] J. R. Lothian, "Some new stylized facts of floating exchange rates," *Journal of International Money and Finance*, vol. 17, no. 1, pp. 29–39, 1998.

[41] Y. Wei, Y. Wang, and D. Huang, "Forecasting crude oil market volatility: Further evidence using GARCH-class models," *Energy Economics*, vol. 32, no. 6, pp. 1477–1484, 2010.

[42] S. Trück and K. Liang, "Modelling and forecasting volatility in the gold market," *International Journal of Banking and Finance*, vol. 9, no. 1, pp. 48–80, 2012.

[43] V. N. Vapnik, *Statistical Learning Theory*. New York: Wiley, 1998.

[44] L. Breiman, "Random forests," *Machine Learning*, vol. 45, no. 1, pp. 5–32, 2001.

[45] K. Theofilatos, S. Likothanassis, and A. Karathanasopoulos, "Modeling and trading the EUR/USD exchange rate using machine learning techniques," *Engineering, Technology & Applied Science Research*, vol. 2, no. 5, pp. 269–272, 2012.

[46] B. Ni, G. Wang, and P. Moulin, "Rgbd-hudaact: A color-depth video database for human daily activity recognition," in *ICCV Workshops*, 2011, pp. 1147–1153.

[47] J. W. Davis and A. F. Bobick, "The representation and recognition of human movement using temporal templates," in *CVPR*, 1997, pp. 928–934.

[48] D. M. Blei and M. I. Jordan, "Variational inference for Dirichlet process mixtures," *Bayesian Analysis*, vol. 1, no. 1, pp. 121–144, 2006.